The Chemical Nature of $Ti_4O_{10}^-$: Vibrational Predissociation Spectroscopy combined with Global Structure Optimization

Fabian Müller,[†,‡] *Joachim Sauer,*[*§] *Xiaowei Song,*[‡,¶] *Knut R. Asmis*[*†]

[†] Wilhelm-Ostwald-Institut für Physikalische und Theoretische Chemie, Universität Leipzig, Linnéstr. 2, 04103 Leipzig, Germany

[‡] Fritz-Haber-Institut der Max-Planck-Gesellschaft, Faradayweg 4-6, 14195 Berlin, Germany

[§] Institut für Chemie, Humboldt-Universität zu Berlin, Unter den Linden 6, 10099 Berlin, Germany

Abstract

The gas phase infrared spectrum of $Ti_4O_{10}^-$ is studied in the spectral range from 400 to 1250 cm^{-1} using cryogenic ion trap vibrational spectroscopy in combination with density functional theory (DFT). The infrared photodissociation (IRPD) spectrum of D_2-tagged $Ti_4O_{10}^-$ provides evidence for a structure of lower symmetry that contains a superoxo group (1121 cm^{-1}) and two terminal Ti=O moieties. DFT combined with a genetic algorithm for global structure optimization predicts two isomers which feature a superoxo group: the C_s symmetric global minimum-energy structure and a similar isomer (C_1) that is slightly higher in energy. Coupled cluster calculations confirm the relative stability. Comparison of the harmonic DFT spectra (different functionals) with the IRPD spectrum suggests that both of these isomers contribute. Earlier assignments to the adamantane-like C_{3v} isomer with three terminal Ti−$O^{\bullet-}$ groups in a quartet state are not confirmed. They were based on the infrared multiple photon photodissociation (IRMPD) spectrum of bare $Ti_4O_{10}^-$ and local DFT structure optimizations.

Introduction

Titanium dioxide is a semiconducting material known for its use in heterogenous catalysis, either as a catalyst or catalyst support. Much interest, for example, has focused on understanding and optimizing its use as a photocatalyst in the water splitting reaction.[1] Nonetheless, there are many open questions as for the nature of the active sites, because they are difficult to study under typical working conditions and spectral assignments are not safe, see, e.g., Refs. 2-5. Gas phase clusters can often serve as model systems for gaining a better understanding in such cases.[6]

Titanium oxide clusters have been studied extensively in the gas phase in recent years (see e.g. Ref. 7 for a summary). Considerable experimental attention has focused on titanium oxide anions, in particular on the way the excess charge influences their structure[7-10] and reactivity[11-15] as a function of cluster size and composition. Theoretical investigations aimed at an elucidation of their structure, stability and optical properties.[16-19] Here, we revisit the geometric and electronic structure of the $Ti_4O_{10}^-$ titanium oxide anion, which may be understood as $O_2^{\bullet-}$ attached to $(TiO_2)_4$ and provide information about oxygen species attached to TiO_2 surfaces.[4, 5]

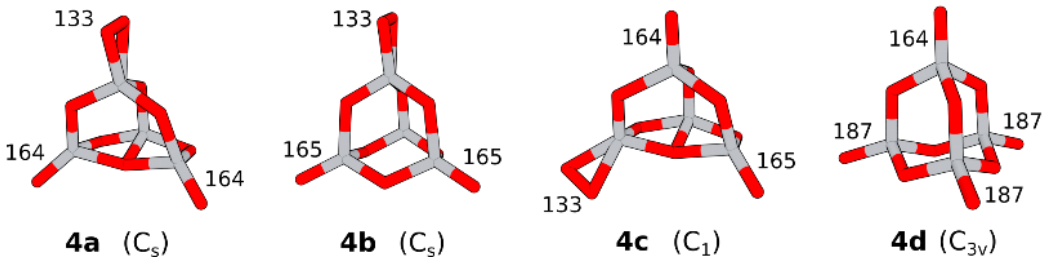

Figure 1. The four lowest TPSSh/def2-TZVPP optimized minimum-energy structures for $Ti_4O_{10}^-$. Bond distances in pm. Titanium atoms are shown in grey, oxygen atoms in red. The nomenclature is taken from Ref. 20.

The vibrational spectrum of $Ti_4O_{10}^-$ was originally obtained by infrared multiple photon photodissociation (IRMPD) spectroscopy in the spectral region from 550 to 1050 cm^{-1}. Based on local structure optimization with density functional theory (DFT), it was assigned to the highly symmetric adamantane-like cage structure **4d**, see Fig. 1. We keep the nomenclature of Ref. 20 for unequivocal reference to previous work. The cage structure **4d** with four terminal oxygen atoms was chosen for local structure optimization as part of the $V_{4-n}Ti_nO_{10}^-$ isomorphous substitution series. Previously, IRMPD studies demonstrated that $(V_2O_5)_n^-$ anions (n = 2–4) form polyhedral cages made of $(–O)_3V{=}O$ units.[21] The $Ti_4O_{10}^-$ cage **4d** instead consists of one $(–O)_3Ti{=}O$ unit and three $(–O)_3Ti{-}O^{\bullet-}$ units, resulting in a quartet spin state. The authors of Ref. 22 have been well aware of the fact that such oxygen-rich transition metal oxide species tend to form superoxo or peroxo units.[22] They indeed found a $Ti_4O_{10}^-$ isomer with a superoxo, $O_2^{\bullet-}$, ligand, but this was 50 kJ mol^{-1} less stable than **4d**.

Later, after a genetic algorithm had proven its ability to find unusual structures of metal oxide clusters such as $Al_8O_{12}^+$ in DFT structure optimizations,[23] a global search for alternative structures of $Ti_4O_{10}^-$ was performed.[20] It yielded structures **4a** – **4c** shown in Fig. 1, which feature a superoxo group each, and which were found up to 68 kJ mol^{-1} more stable than **4d** using DFT.

$Ti_4O_{10}^-$ is an example of "overoxidation". In a "stoichiometric" Ti_4O_8 cluster, each titanium atom would be fully oxidized to Ti^{4+} and each oxygen atom fully reduced to O^{2-} which can be written in a fully ionic picture as $[(Ti^{4+})_4(O^{2-})_8]$. For the two additional oxygen atoms in $Ti_4O_{10}^-$ = $[Ti_4O_8][O_2]^-$ there is just the additional electron of the anion available for reduction. One possibility is that they form a superoxo species ($O_2^{\bullet-}$) as in **4a** – **4c**, which can be written in a fully ionic picture as $[(Ti^{4+})_4(O^{2-})_8](O_2^{\bullet-})$. The other possibility is to distribute the electron

deficiency more equally, leading to three $O^{\bullet-}$ ions as in **4d**, with $[(Ti^{4+})_4(O^{2-})_7]^{2+}(O^{\bullet-})_3$. That **4d** is much less stable than **4a** – **4c** is another example for "inequality creates stability" which we had found before for cationic and neutral Al_8O_{12}.[23] A more general phenomenon of this type is the Jahn-Teller effect.

The IR spectra of **4a** – **4c** are predicted to exhibit a characteristic band slightly above 1200 cm^{-1} (1202-1208 cm^{-1}) due to excitation of the O-O stretching mode of the $O_2^{\bullet-}$ group. A corresponding band was not observed in the original IRMPD study. While the primarily reported spectrum[22] only extended up to 1050 cm^{-1}, overview spectra were indeed measured up to 1400 cm^{-1} as part of the original study and these showed no photodissociation signal above 1000 cm^{-1}. Analysis of the spectrum up to 1050 cm^{-1} led to the conclusion that the experimental IRMPD spectrum was due to a mixture of **4b** and **4d** dominated by the adamantane-like cage **4d**.[20] Observation of this high energy isomer was suggested to be due to kinetic trapping in the cluster preparation process which is not very likely. For the experimental setup in question it has only been reported for such cases, where special measures were taken to greatly enhance kinetic trapping.[24]

To unravel the discrepancies between experiment and theory, here we revisit the gas phase vibrational spectrum of $Ti_4O_{10}^-$ over a broad spectral range, including the superoxo stretching region. We use messenger-tagging with D_2 to obtain vibrational predissociation spectra of $Ti_4O_{10}^-\cdot D_2$ in the linear absorption regime, which we refer to as IRPD (vs. IRMPD) spectra. We then compare this spectrum to the original IRMPD spectrum[22] of bare $Ti_4O_{10}^-$, commenting on common pitfalls in the assignment of such spectra. We assign the obtained IRPD spectra based on a comparison with harmonic IR spectra from DFT calculations. We also discuss the advantages and limitations of the cosine similarity score[25] as criterion for the assignment of the

vibrational spectra. For a safe structure determination, the structure that yields the best agreement with the spectrum should also have the lowest energy. Here we go beyond DFT which cannot be systematically improved and use coupled cluster theory to calculate improved energies at the DFT structures ("single-point energies").

Experimental Methods

Infrared photodissociation (IRPD) experiments were conducted on an ion trap tandem mass spectrometer described previously.[26, 27] Titanium oxide anions were produced using a Smalley-type[28] laser vaporization ion source.[14, 29] The second harmonic output (532 nm, ~10 mJ) of a Nd:YAG laser (Litron, Nano S) operated at 50 Hz was focused onto the surface of a rotating and translating titanium rod. The resulting plasma is entrained in a pulse of 0.75% O_2 seeded in He carrier gas (backing pressure: 6 bar) and expanded through a clustering channel held at 270 K. The ion beam passes through a 4 mm skimmer, is then collimated in a radio frequency (RF) decapole ion guide filled with He gas and mass-selected using a quadrupole mass-filter. The beam is then deflected by 90° with an electrostatic quadrupole ion deflector and focused into a RF ring-electrode ion-trap, held at 15 K and continuously filled with pure D_2 gas. Trapped ions are accumulated, thermalized, and messenger-tagged[30] through collisions with the buffer gas.

All ions are extracted from the trap at 5 Hz and are focused into the center of the extraction region of an orthogonal time-of-flight (TOF) mass spectrometer. Here, the ion packet is irradiated with a single Fritz Haber Institute Free-Electron Laser (FHI FEL) macropulse (~10 μs pulse length). The FHI FEL is tuned from 400 to 1200 cm^{-1} with a bandwidth of ca. 0.3% root mean square of the central wavelength and pulse energies of ~0.1 to 2 mJ. The TOF intensities of all ions are monitored simultaneously as the FEL wavelength is scanned from 400 to 1200 cm^{-1}

in 3 cm^{-1} steps; for each wavelength step, ~30 TOF traces are acquired and averaged. Typically, at least three scans are summed, the photodissociation cross section σ_{IRPD} is determined as described previously,[31, 32] and the data obtained in separately scanned ranges are stitched together to obtain the final IRPD spectrum.

Computational Methods

DFT and coupled cluster calculations using the Turbomole program package 7.3[33, 34] were done for four low energy isomers identified by a genetic algorithm in a former study.[20] All structures were re-optimized with DFT employing a triple-zeta basis set with polarization functions (def2-TZVPP).[35, 36] Simulated IR spectra result from harmonic vibrational frequency calculations based on analytical second derivatives.[37] Three different exchange-correlation functionals were employed: PBE[38, 39] (generalized gradient approximation, GGA), B3LYP[40-42] (hybrid-GGA) and TPSSh[43] (hybrid-meta-GGA).

Coupled cluster numbers rely on unrestricted Hartree-Fock (UHF) reference functions and include single, double and perturbative triple substitutions, labeled CCSD(T).[44] Single point calculations with the def2-TZVPP basis set were done at the TPSSh structures. All calculations made use of the resolution of the identity approximation for the evaluation of the Coulomb term (RI-J).[45, 46]

For a better comparison with the experimental findings, the calculated stick spectra were convoluted with Gaussian line shapes with a full width at half maximum (FWHM) of 15 cm^{-1} and the cosine similarity score,[25] *S*, for the agreement between a particular simulated spectrum and the IRPD result was calculated as in previous studies:[47, 48]

$$S = \cos(\theta) = \frac{\langle A,B \rangle}{\|A\|\|B\|} = \frac{\sum_{i=1}^{n} A_i B_i}{\sqrt{\sum_{i=1}^{n} A_i^2}\sqrt{\sum_{i=1}^{n} B_i^2}} \quad (1)$$

The vectors *A* and *B* contain the normalized calculated and measured IR intensities, respectively, sampled on the same wavelength grid. *S* can be interpreted as the normalized cross-correlation of *A* and *B* with a displacement of zero, or as their normalized discrete overlap integral. In principle, it can take values between −1 and 1, but only values between 0 and 1 appear in application since the IR intensities in *A* and *B* are all positive.

The influence of the D_2 tag on the DFT spectra is shown in Fig. S1. Except for a slight shift of a band around 600 cm^{-1} in the spectrum of **4c** no significant changes occur. Hence, all shown calculated spectra and energies refer to the untagged isomers.

Results

The IRPD spectrum of D_2-tagged $Ti_4O_{10}^-$ is given in Fig. 2B. In the spectral region from 400 to 1250 cm^{-1} it shows more than 13 features, which are labeled with A to N. Band positions and assignments are listed in Table 1. The highest energy feature is found at 1121 cm^{-1} (A). Its position together with a low IR intensity is characteristic for the presence of a superoxo group.[49] Next in energy are two more intense bands at 986 cm^{-1} (B) and 968 cm^{-1} (C), a region that is associated with terminal titanium oxo bonds (Ti=O).[7] Most of the IR activity is observed between 890 cm^{-1} and 780 cm^{-1} yielding a series of four bands (D-G) of which band F is the broadest (~30 cm^{-1} FWHM) and also the most intense of all observed bands. Below 750 cm^{-1} at least six narrower (5-15 cm^{-1}) and less intense IR peaks (H-N) are observed. Their width is limited by the spectral width of the excitation laser, confirming that the D_2-tagged $Ti_4O_{10}^-$ are sufficiently cold. Summarizing, the larger number of IR active bands is rather surprising in the light of the much simpler previously predicted IR spectra.[20, 22] Clearly, the present IR spectrum

cannot be exclusively associated with a highly symmetric species like **4d** that was originally assigned based on a comparison to the IRMPD spectrum of bare $Ti_4O_{10}^-$, depicted in Fig. 2A.

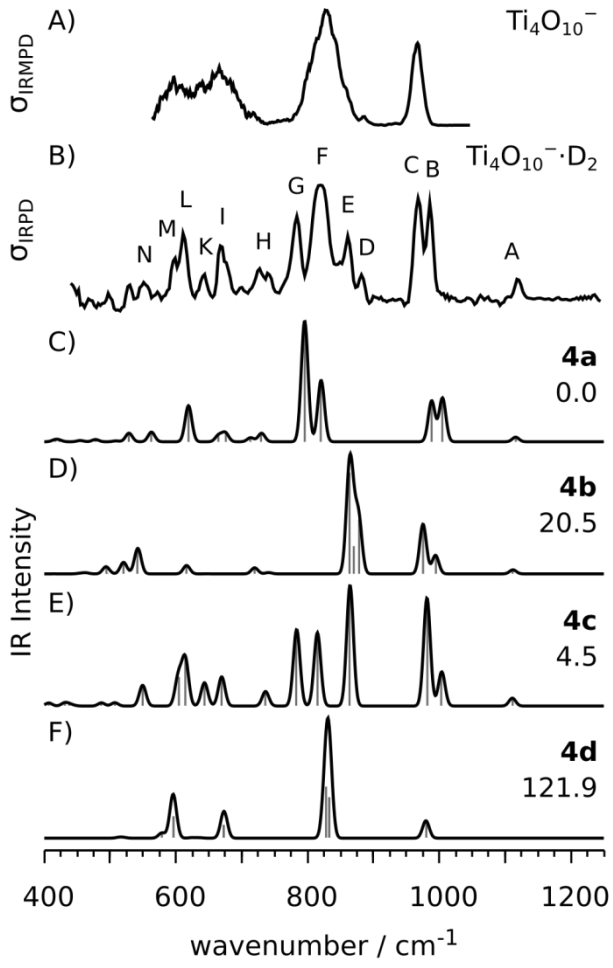

Figure 2. Comparison of (A) the IRMPD of bare $Ti_4O_{10}^-$ (from Ref. 22) and (B) the IRPD spectrum of D_2-tagged $Ti_4O_{10}^-$ (present study) to the calculated spectra (C-F) of the four most stable isomers **4a** – **4d**. The relative CCSD(T) energies are given in kJ mol^{-1} (see Table 2). The superoxo band of the calculated spectra was scaled with the factor 0.9356.

Comparison of the present, well-resolved IRPD spectrum of D_2-tagged $Ti_4O_{10}^-$ to the previously measured, rather structureless IRMPD spectrum of bare $Ti_4O_{10}^-$ yields some additional insights. Note, IR absorption is observed in similar (but not identical) spectral regions in both types of spectra. Namely, the IRPD bands B and C (1000-950 cm^{-1}), D to G (890-750 cm^{-1}) and H to M (750-560 cm^{-1}) correlate well with the three main IRMPD features extending from 990-940 cm^{-1}, 990-770 cm^{-1} and 730-560 cm^{-1}. Also, the relative intensities of these three features mimic the overall IRPD intensities pattern, suggesting that indeed the same $Ti_4O_{10}^-$ species was probed in the two experiments. However, band A can only be found in the IRPD spectrum. The spectral range up to 1400 cm^{-1} was taken into consideration in the primary IRMPD measurements and no IR absorption was found above 1000 cm^{-1}.

Differences in the two spectra are related predominantly to the different dissociation channels monitored, D_2-loss (IRPD) vs. TiO_3-loss (IRMPD), and hence the amount of energy that needs to be absorbed to induce photodissociation. In the IRPD case, $Ti_4O_{10}^-\cdot D_2 \rightarrow Ti_4O_{10}^- + D_2$ requires less than 8 kJ mol^{-1}, while the IRMPD case, $Ti_4O_{10}^- \rightarrow Ti_3O_7^- + TiO_3$, requires more than 250 kJ mol^{-1}, probably up to 500 kJ mol^{-1}. Only the messenger technique therefore allows to probe in the linear absorption spectrum over large parts of the IR spectral range, while the cross section measured in the IRMPD experiment is governed by the nature of the multiple photon absorption process.[50, 51] This can lead to significant discrepancies between the measured IRMPD vs. the calculated IR intensities. Band A (superoxo stretching) is an example for such a discrepancy, sometimes referred to as a so-called IRMPD-transparent band,[31, 52] which typically results from a change in the fundamental frequency upon heating,[27] a change in the transition dipole moment upon heating,[53] the presence of uncoupled oscillators[54] or also non-statistical mode-specific fragmentation.[55] Consequently, such effects, which were not fully understood at the time of

publication of the original IRMPD spectrum, need to be considered when making structure assignments based on the analysis of IRMPD bands which involve the absorption of many IR photons.

The difference in the average internal energy content of the ions prior to IR irradiation also needs to be considered. Note, the ion trap temperature (IRMPD: 17 K, IRPD: 15 K) and buffer gas pressure are similar in the two experiments, suggesting similar ion internal energies. However, formation (and dissociation) of messenger complexes in the present experiment results in an additional cooling mechanism, yielding colder ions as well as preventing hotter ones from being probed.[31, 32] Thus, the slightly hotter ensemble in the original experiment may also contribute to broadening of the IRMPD bands.

Table 1. Harmonic TPSSh/def2-TZVPP vibrational frequencies (in cm^{-1}) of four $Ti_4O_{10}^-$ isomers grouped according to the nature of the normal modes.[a] Experimental vibrational frequencies (cm^{-1}) are also shown and assigned accordingly.

Isomer/ Spectrum	**O–O stretching**[a]	**Ti=O$_t$ stretching**	**$\mu_{2/3}$-O stretching & bending**	**O$_2$…(Ti$_4$O$_8$) stretching**
4a	1116	1005, 988	821, 796, 730, 713, 675, 665, 619, 563	529
4b	1112	994, 975	877, 869, 864, 741, 720, 647, 616, 542	520
4c	1111	1004, 981	864, 815, 783, 736, 670, 643, 614, 604	549
4d		980	832, 828, 673, 636,[d] 625,[d] 596, 579	
IRPD[b]	1121 (A)	986 (B), 968 (C)	882 (D), 864 (E), 819 (F), 784 (G), 742 (H), 676 (I), 644 (K), 614 (I), 596 (M)	554 (N)
IRMPD[c]		967	885, 828, 718, 666, 597	

[a] Scaled with f = 0.9356 derived from gas phase O_2^-, see SI, Tab. S1. [b] Present study. [c] From Ref. 22. [d] Ti–$O_t^{\bullet}$ stretching

For the structure determination of the $Ti_4O_{10}^-$ cluster based on the present IRPD spectrum the same low energy isomers (Fig. 1) were taken into account that were used in the previous assignment of the IRMPD spectrum.[20] Their calculated IR spectra (TPSSh/def2-TZVPP) are shown in Fig. 2C – F (see Fig. S3 for B3LYP results). Consideration of the D_2 tag leaves the IR spectra nearly unchanged (cf. Fig. S1). The relative stabilities (Table 2) of the four isomers were determined with three different exchange-correlation functionals (B3LYP, PBE and TPSSh) and with CCSD(T). For all considered systems, the T_1, D_1 and %TAE diagnostics[56] are well below the thresholds for non-negligible multi-referential character (Tab. S1) due to almost empty Ti d-shells. This allows for a reliable treatment with single-reference methods such as coupled cluster.

CCSD(T) predicts isomer **4a** to be the global minimum-energy structure, closely followed by **4c** (+5 kJ mol^{-1}). DFT agrees on the global minimum; the difference to **4c** is overestimated by 2 – 4 kJ mol^{-1} only. For the stability difference between the **4d** structure with three Ti−$O^{\bullet-}$ bonds and **4a**, CCSD(T) yields a much larger value (122 kJ mol^{-1}) than B3LYP (71 kJ mol^{-1}) which was used in the previous $Ti_4O_{10}^-$ studies.[20, 22] The increasing deviations of PBE, TPSSh, and B3LYP from CCSD(T), −2, −21, and −51 kJ mol^{-1}, respectively, follow the increasing admixture of Fock exchange (0%, 10%, and 20%, respectively) which favors localized electrons (radicals).

Table 2. Relative energies (kJ mol^{-1}) of isomers **4a** – **4d** of $Ti_4O_{10}^-$ obtained with the B3LYP, PBE and TPSSh functionals. Energies including zero-point vibrational energies are given in

parenthesis when available. CCSD(T) numbers are single point calculations at the TPSSh structures. Basis set: def2-TZVPP.

Iso	State	B3LYP		PBE		TPSSh		CCSD(T)
4a	^{2}A" (C_s)	0	(0)	0	(0)	0	(0)	0
4b	^{2}A" (C_s)	3	(3)	10	(10)	23	(23)	20
4c	^{2}A (C_1)	8	(8)	7	(7)	9	(10)	5
4d	^{4}E (C_{3v})	71	(64)	120	(106)	101	(94)	122
4d	^{2}A (C_1)	71	(64)	124	(110)	102	(94)	122

The calculated IR spectra of the energetically disfavored isomers **4b** and **4d** (Figs. 2D and 2F, respectively) feature a rather small number of intense bands due to the high symmetry of their basic cage structure. This does not agree with the measured IRPD spectrum. Neither **4b** nor **4d**, for instance, can account for band G. Although it cannot be ruled out that both isomers have a minor contribution to the measured spectrum, the overall appearance of the spectrum is reproduced neither by each of them alone nor by a mixture of both as was suggested previously.[20]

The IR spectrum of the most stable isomer **4a**, instead, is a much better fit with respect to both band position and intensity (cf. Fig. 2 and Table 1). However, bands D and E are not reproduced. A similar picture arises for the predicted spectrum of **4c**: except for band D there is agreement with the measurement. Unlike **4a**, there are some mismatches concerning the intensity ratios between the bands, especially the predicted intensities of bands E (too high) and B (to low) differ from the experiment. Comparing IRPD bands B and C, however, reveals that C is broader than B indicating an intensity difference of both signals in line with the DFT calculation.

Based on previous experience[49, 57, 58] the frequency of the superoxo stretching band of **4a**, **4b** and **4c** has been scaled with a factor 0.9356 derived from gas phase O_2^-, see SI, Table S1. Frequency scaling is common practice to account for systematic errors of quantum chemical force constant calculations. Hybrid functionals as used here yield too short bonds and too large harmonic force constants and, hence, require scale factors smaller than one.[59, 60] After scaling, the superoxo frequencies predicted for **4a**, **4b** and **4c** agree within 10 cm^{-1} with experiment (1121 cm^{-1}, band A).

Table 3. Cosine similarity scores of the IRPD spectrum and the calculated spectra of the isomers **4a** – **4d** obtained with TPSSh and B3LYP (unscaled wavenumbers, def2-TZVPP).

Iso	TPSSh	B3LYP
4a	0.52	0.45
4b	0.33	0.32
4c	0.73	0.64
4d	0.51	0.28

A quantitative measure of the similarity of the predicted and the IRPD spectra is the cosine similarity score, which is the normalized discrete overlap of the two considered spectra (see section Computational Methods for details). It can take values between 0 and 1, where 1 means perfect agreement. Table 3 shows the scores for the IRPD spectrum (this work) and Table S2 those for the IRMPD[22] spectrum. The former is compared to the unscaled TPSSh and B3LYP spectra reported in this work. For the latter one the scores are given for the B3LYP spectra

obtained in the former studies (Refs. 20, 22). The superoxo band was not included when calculating the scores.

At the TPSSh level **4c** reaches the highest score with a value of 0.73, followed by **4a** with 0.52. The match between **4d** and the IRPD spectrum is similar to the one of **4a** with a value of 0.51 and the least similarity is found for **4b** with only 0.32. By global scaling of the TPSSh wavenumbers with a factor between 0.9 and 1.1 in order to maximize the score, the qualitative picture is retained. Since the "optimal" global scaling factor would be 0.99 we decided to stick to the unscaled TPSSh spectra. The B3LYP results for **4b** and **4d** show even less agreement between experiment and calculation. The slightly smaller scores for **4c** and **4a** compared to TPSSh result from the small blue-shift of all signals (away from the experimental band positions) due to the higher amount of admixed Fock-exchange in B3LYP and the resulting increase of the force constants.

A plot of the cosine similarity score of the four isomers against the wavenumber can be found in Fig. S4. It illustrates why the spectrum of isomer **4c** exhibits the highest score: it shows agreement across large parts of the IR spectral range probed, while the spectra of the other isomers only agree in narrower spectral ranges. The figure also demonstrates that the highest energy band, which is assigned to the superoxo species, does not contribute to the score when it is unscaled. This exemplifies the limits of this very simple indicator: the “chemically” most characteristic band in the spectrum cannot be considered. Moreover, its use in conjunction with IRMPD spectra is less reliable than with IRPD spectra. For example, the scoring with respect to the IRMPD spectrum is severely affected by the application of a global scaling factor to the calculated wavenumbers as can be seen in Table S3: global scaling leads to a complete reversal

of the order of scores for the agreement of the IRMPD spectrum with the B3LYP/def2-TZVP calculations.

Overall, the current IRPD spectrum of $Ti_4O_{10}^-\cdot D_2$ shows a rich structure pointing to low spatial symmetry. The comparison with the DFT spectra and relative stabilities of **4a** – **4d** confirms this assumption: the highly symmetric (C_{3v}) tri-radical **4d** is not only much higher in energy than the C_s/C_1 isomers **4a**/**4c**. It also has a very limited number of IR signals, in clear disagreement with the experiment. Whereas the IRPD spectrum shows better agreement with the prediction for isomer **4c** than for **4a** (Fig. 2 and Table 3), isomer **4a** is slightly more stable than **4c** (Table 2). However, the energy difference of 7 – 9 kJ mol^{-1} for DFT and 5 kJ mol^{-1} for CCSD(T), see Table 2, is within the uncertainty limits of the calculations. It is also possible that both isomers coexist in experiment, which would result in a superposition of their IR features. The TPSSh spectrum for a 50:50 mixture (Fig. S2) reaches a cosine similarity score of 0.71, close to the value of **4c** alone (0.73, Table 3). Hence, it remains undecided which of the closely related superoxo structures **4a** and **4c** dominates in the observed IRPD spectrum, or if it results from an even mixture. But there is no doubt that the species in question contain a terminal η^2-superoxo group, a fact on which experiment and theory agree.

Conclusion

Progress in natural science comes with new methods. Our study shows that passing in experiment from multiple photon dissociation of the bare anion to single photon dissociation of the messenger-tagged anion, and in theory from local optimization of "intelligent design" structure models to global structure optimization with an genetic algorithm changes the assignment of the $Ti_4O_{10}^-$ structure from a symmetric tetrahedral cage with terminal titanium-

oxygen bonds (one Ti=O, three Ti−$O^{\bullet-}$) to a less symmetric cage with two terminal Ti=O bonds and one terminal superoxo species. At the current resolution of the IRPD spectra and the uncertainty of the currently applicable quantum chemical methodology, an unambiguous assignment to a single isomer is not yet possible.

ASSOCIATED CONTENT

Supporting Information

The following supporting information is available free of charge at https://pubs.acs.org/...

Figures depicting the influence of D2-tagging on the TPSSh spectra and B3LYP results, a table with cosine similarity scores for B3LYP vs. IRMPD, figures showing the decomposition of the scores, a table with all absolute energies from PBE, B3LYP, TPSSh, UHF and CCSD(T). (PDF)

Cartesian coordinates for all isomers optimized with PBE, TPSSh and B3LYP. (XLSX)

AUTHOR INFORMATION

Corresponding Author

* js@chemie.hu-berlin.de

* knut.asmis@uni-leipzig.de

ORCID

Fabian Müller: 0000-0002-1774-6373

Joachim Sauer: 0000-0001-6798-6212

Xiaowei Song: 0000-0002-5820-7763

Knut Asmis: 0000-0001-6297-5856

Present Addresses

¶ IKEA of Sweden AB, SE-343 34 Almhult, Sweden

Author Contributions

The manuscript was written through contributions of all authors. All authors have given approval to the final version of the manuscript.

Notes

The authors declare no competing financial interests.

ACKNOWLEDGMENT

We thank Matias R. Fagiani and Sreekanta Debnath for their help with measuring the IRPD spectrum. This work has been funded by Deutsche Forschungsgemeinschaft (DFG, German Research Foundation) within the project 430942176 (Asmis/Sauer). X.S. gratefully acknowledges an Alexander-von-Humboldt Foundation post-doctoral research fellowship.

REFERENCES

1. Miyoshi, A.; Nishioka, S.; Maeda, K., Water Splitting on Rutile TiO2-Based Photocatalysts. *Chem. Eur. J.* **2018,** *24* (69), 18204-18219.

2. Beck, T. J.; Klust, A.; Batzill, M.; Diebold, U.; Di Valentin, C.; Selloni, A., Surface Structure of TiO2(011)(2x1). *Phys. Rev. Lett.* **2004,** *93* (3), 036104.

3. Gong, X.-Q.; Khorshidi, N.; Stierle, A.; Vonk, V.; Ellinger, C.; Dosch, H.; Cheng, H.; Selloni, A.; He, Y.; Dulub, O.; et al., The 2×1 reconstruction of the rutile TiO2(011) surface: A combined density functional theory, X-ray diffraction, and scanning tunneling microscopy study. *Surf. Sci.* **2009,** *603* (1), 138-144.

4. Cheng, J.; VandeVondele, J.; Sprik, M., Identifying Trapped Electronic Holes at the Aqueous TiO2 Interface. *J. Phys. Chem. C* **2014,** *118* (10), 5437-5444.

5. Petrik, N. G.; Kimmel, G. A., Photoinduced Dissociation of O2 on Rutile TiO2(110). *J. Phys. Chem. Lett.* **2010,** *1* (12), 1758-1762.

6. Sauer, J.; Freund, H.-J., Models in Catalysis. *Catal. Lett.* **2015,** *145* (1), 109-125.

7. Weichman, M. L.; Song, X.; Fagiani, M. R.; Debnath, S.; Gewinner, S.; Schöllkopf, W.; Neumark, D. M.; Asmis, K. R., Gas phase vibrational spectroscopy of cold (TiO2)n− (n = 3–8) clusters. *J. Chem. Phys.* **2016,** *144* (12), 124308.

8. Wu, H.; Wang, L. S., Electronic structure of titanium oxide clusters: TiOy (y = 1−3) and (TiO2)n (n = 1−4). *J. Chem. Phys.* **1997,** *107* (20), 8221-8228.

9. Zhai, H.-J.; Wang, L.-S., Probing the Electronic Structure and Band Gap Evolution of Titanium Oxide Clusters (TiO2)n- (n = 1−10) Using Photoelectron Spectroscopy. *J. Am. Chem. Soc.* **2007,** *129* (10), 3022-3026.

10. Kim, J. B.; Weichman, M. L.; Neumark, D. M., Structural Isomers of Ti2O4 and Zr2O4 Anions Identified by Slow Photoelectron Velocity-Map Imaging Spectroscopy. *J. Am. Chem. Soc.* **2014,** *136* (19), 7159-7168.

11. Debnath, S.; Song, X.; Fagiani, M. R.; Weichman, M. L.; Gao, M.; Maeda, S.; Taketsugu, T.; Schöllkopf, W.; Lyalin, A.; Neumark, D. M.; et al., CO2 Adsorption on Ti3O6–: A Novel Carbonate Binding Motif. *J. Phys. Chem. C* **2019,** *123* (13), 8439-8446.

12. Debnath, S.; Song, X.; Fagiani, M. R.; Weichman, M. L.; Gao, M.; Maeda, S.; Taketsugu, T.; Schöllkopf, W.; Lyalin, A.; Neumark, D. M.; et al., Correction to "CO2 Adsorption on Ti3O6–: A Novel Carbonate Binding Motif". *J. Phys. Chem. C* **2020,** *124* (12), 6952-6953.

13. Lv, S. Y.; Liu, Q. Y.; Zhao, Y. X.; He, S. G., Photooxidation of Isoprene by Titanium Oxide Cluster Anions with Dimensions up to a Nanosize. *J. Am. Chem. Soc.* **2021,** *143* (10), 3951-3958.

14. Song, X.; Fagiani, M. R.; Debnath, S.; Gao, M.; Maeda, S.; Taketsugu, T.; Gewinner, S.; Schöllkopf, W.; Asmis, K. R.; Lyalin, A., Excess charge driven dissociative hydrogen adsorption on Ti2O4−. *Phys. Chem. Chem. Phys.* **2017,** *19* (34), 23154-23161.

15. Weichman, M. L.; Debnath, S.; Kelly, J. T.; Gewinner, S.; Schöllkopf, W.; Neumark, D. M.; Asmis, K. R., Dissociative Water Adsorption on Gas-Phase Titanium Dioxide Cluster Anions Probed with Infrared Photodissociation Spectroscopy. *Top. Catal.* **2018,** *61* (1), 92-105.

16. Hamad, S.; Catlow, C. R.; Woodley, S. M.; Lago, S.; Mejias, J. A., Structure and stability of small TiO2 nanoparticles. *J. Phys. Chem. B* **2005,** *109* (33), 15741-8.

17. Li, S.; Dixon, D. A., Molecular structures and energetics of the (TiO2)n (n = 1-4) clusters and their anions. *J. Phys. Chem. A* **2008,** *112* (29), 6646-66.

18. Chen, M.; Dixon, D. A., Tree Growth-Hybrid Genetic Algorithm for Predicting the Structure of Small (TiO2)n, n = 2-13, Nanoclusters. *J. Chem. Theory Comput.* **2013,** *9* (7), 3189-200.

19. Shevlin, S. A.; Woodley, S. M., Electronic and Optical Properties of Doped and Undoped (TiO2)n Nanoparticles. *J. Phys. Chem. C* **2010,** *114* (41), 17333-17343.

20. Helmich, B.; Sierka, M.; Döbler, J.; Sauer, J., Structure and properties of bimetallic titanium and vanadium oxide clusters. *Phys. Chem. Chem. Phys.* **2014,** *16* (18), 8441-7.

21. Asmis, K. R.; Santambrogio, G.; Brümmer, M.; Sauer, J., Polyhedral Vanadium Oxide Cages: Infrared Spectra of Cluster Anions and Size-Induced d Electron Localization. *Angew. Chem. Int. Ed.* **2005,** *44* (20), 3122-3125.

22. Janssens, E.; Santambrogio, G.; Brummer, M.; Woste, L.; Lievens, P.; Sauer, J.; Meijer, G.; Asmis, K. R., Isomorphous substitution in bimetallic oxide clusters. *Phys. Rev. Lett.* **2006,** *96* (23), 233401.

23. Sierka, M.; Döbler, J.; Sauer, J.; Santambrogio, G.; Brümmer, M.; Wöste, L.; Janssens, E.; Meijer, G.; Asmis, K. R., Unexpected structures of gas phase aluminium oxide clusters. *Angew. Chem. Int. Ed.* **2007,** *46*, 3372-3375.

24. Esser, T. K.; Knorke, H.; Siro-Brigiano, F.; Galimberti, D. R.; Asmis, K. R.; Gaigeot, M.-P.; Lisy, J. M., Influence of argon and D2 tagging on the hydrogen bond network in Cs+(H2O)3; kinetic trapping below 40 K. *Phys. Chem. Chem. Phys.* **2018,** *20* (45), 28476-28486.

25. Kempkes, L. J. M.; Martens, J.; Berden, G.; Houthuijs, K. J.; Oomens, J., Investigation of the position of the radical in z3-ions resulting from electron transfer dissociation using infrared ion spectroscopy. *Faraday Discuss.* **2019,** *217* (0), 434-452.

26. Goebbert, D. J.; Asmis, K. R.; Meijer, G., 10 K Ring Electrode Trap--Tandem Mass Spectrometer for Infrared Spectroscopy of Mass Selected Ions. *AIP Conf. Proc.* **2009,** *1104*, 22-29.

27. Goebbert, D. J.; Garand, E.; Wende, T.; Bergmann, R.; Meijer, G.; Asmis, K. R.; Neumark, D. M., Infrared spectroscopy of the microhydrated nitrate ions NO(3)(-)(H2O)(1-6). *J. Phys. Chem. A* **2009,** *113* (26), 7584-92.

28. Duncan, M. A., Invited review article: laser vaporization cluster sources. *Rev. Sci. Instrum.* **2012,** *83* (4), 041101.

29. Wende, T. Gas Phase Infrared Photodissociatrion Spectroscopy of Mass-Selected Ionic Clusters. Freie Universität Berlin, Berlin, 2012.

30. Asmis, K. R.; Wende, T.; Brummer, M.; Gause, O.; Santambrogio, G.; Stanca-Kaposta, E. C.; Dobler, J.; Niedziela, A.; Sauer, J., Structural variability in transition metal oxide clusters: gas phase vibrational spectroscopy of V3O(6-8)+. *Phys. Chem. Chem. Phys.* **2012,** *14* (26), 9377-88.

31. Heine, N.; Asmis, K. R., Cryogenic ion trap vibrational spectroscopy of hydrogen-bonded clusters relevant to atmospheric chemistry. *Int. Rev. Phys. Chem.* **2015,** *34* (1), 1-34.

32. Heine, N.; Asmis, K. R., Cryogenic Ion Trap Vibrational Spectroscopy of Hydrogen-Bonded Clusters Relevant to Atmospheric Chemistry (International Reviews in Physical Chemistry, 2015, Vol. 34, No. 1, 1–34). *Int. Rev. Phys. Chem.* **2016,** *35* (3), 507-507.

33. *TURBOMOLE V7.3, a development of University of Karlsruhe and Forschungszentrum Karlsruhe GmbH, 1989-2007, TURBOMOLE GmbH, since 2007; available from http://www.turbomole.com*, 2018.

34. Ahlrichs, R.; Bär, M.; Häser, M.; Horn, H.; Kölmel, C., Electronic structure calculations on workstation computers: The program system turbomole. *Chem. Phys. Lett.* **1989,** *162* (3), 165-169.

35. Weigend, F., Accurate Coulomb-fitting basis sets for H to Rn. *Phys. Chem. Chem. Phys.* **2006,** *8* (9), 1057-1065.

36. Weigend, F.; Ahlrichs, R., Balanced basis sets of split valence, triple zeta valence and quadruple zeta valence quality for H to Rn: Design and assessment of accuracy. *Phys. Chem. Chem. Phys.* **2005,** *7*, 3297-3305.

37. Deglmann, P.; Furche, F.; Ahlrichs, R., An efficient implementation of second analytical derivatives for density functional methods. *Chem. Phys. Lett.* **2002,** *362* (5-6), 511-518.

38. Perdew, J. P.; Burke, K.; Ernzerhof, M., Generalized Gradient Approximation Made Simple. *Phys. Rev. Lett.* **1996,** *77* (18), 3865-3868.

39. Perdew, J. P.; Burke, K.; Ernzerhof, M., Generalized Gradient Approximation Made Simple [Phys. Rev. Lett. 77, 3865 (1996)]. *Phys. Rev. Lett.* **1997,** *78* (7), 1396-1396.

40. Becke, A. D., Density-functional thermochemistry. III. The role of exact exchange. *J. Chem. Phys.* **1993,** *98* (7), 5648-5652.

41. Lee, C.; Yang, W.; Parr, R. G., Development of the Colle-Salvetti correlation-energy formula into a functional of the electron density. *Phys. Rev. B* **1988,** *37* (2), 785-789.

42. Vosko, S. H.; Wilk, L.; Nusair, M., Accurate spin-dependent electron liquid correlation energies for local spin density calculations: a critical analysis. *Can. J. Phys.* **1980,** *58* (8), 1200-1211.

43. Staroverov, V. N.; Scuseria, G. E.; Tao, J.; Perdew, J. P., Comparative assessment of a new nonempirical density functional: Molecules and hydrogen-bonded complexes. *J. Chem. Phys.* **2003,** *119* (23), 12129-12137.

44. Tew, D. P.; Klopper, W.; Neiss, C.; Hattig, C., Quintuple-zeta quality coupled-cluster correlation energies with triple-zeta basis sets. *Phys. Chem. Chem. Phys.* **2007,** *9* (16), 1921-30.

45. Weigend, F., A fully direct RI-HF algorithm: Implementation, optimised auxiliary basis sets, demonstration of accuracy and efficiency. *Phys. Chem. Chem. Phys.* **2002,** *4* (18), 4285-4291.

46. Ahlrichs, R., Efficient evaluation of three-center two-electron integrals over Gaussian functions. *Phys. Chem. Chem. Phys.* **2004,** *6* (22).

47. Müller, F.; Stückrath, J. B.; Bischoff, F. A.; Gagliardi, L.; Sauer, J.; Debnath, S.; Jorewitz, M.; Asmis, K. R., Valence and Structure Isomerism of Al2FeO4+: Synergy of Spectroscopy and Quantum Chemistry. *J. Am. Chem. Soc.* **2020,** *142* (42), 18050-18059.

48. Mayer, M.; Asmis, K. R., Online Monitoring of Isomeric Reaction Intermediates. *J. Phys. Chem. A* **2021,** *125* (14), 2801-2815.

49. Asmis, K. R.; Sauer, J., Mass-selective Vibrational Spectroscopy of Vanadium Oxide Cluster Ions. *Mass Spectrom. Rev.* **2007,** *26*, 542-62.

50. Oomens, J.; Sartakov, B. G.; Meijer, G.; von Helden, G., Gas-phase infrared multiple photon dissociation spectroscopy of mass-selected molecular ions. *Int. J. Mass. Spectrom.* **2006,** *254*, 1-19.

51. Oomens, J.; van Roij, A. J. A.; Meijer, G.; von Helden, G., Gas-Phase Infrared Photodissociation Spectroscopy of Cationic Polyaromatic Hydrocarbons. *Astrophys. J.* **2000,** *542*, 404.

52. Asmis, K. R., Structure characterization of metal oxide clusters by vibrational spectroscopy: possibilities and prospects. *Phys. Chem. Chem. Phys.* **2012,** *14* (26), 9270-9281.

53. Heine, N.; Yacovitch, T. I.; Schubert, F.; Brieger, C.; Neumark, D. M.; Asmis, K. R., Infrared photodissociation spectroscopy of microhydrated nitrate-nitric acid clusters NO3(-)(HNO3)(m)(H2O)(n). *J. Phys. Chem. A* **2014,** *118* (35), 7613-22.

54. Beck, J. P.; Lisy, J. M., Infrared spectroscopy of hydrated alkali metal cations: evidence of multiple photon absorption. *J. Chem. Phys.* **2011,** *135* (4), 044302.

55. Pankewitz, T.; Lagutschenkov, A.; Niedner-Schatteburg, G.; Xantheas, S. S.; Lee, Y. T., Infrared spectrum of NH4+(H2O): evidence for mode specific fragmentation. *J. Chem. Phys.* **2007,** *126* (7), 074307.

56. Jiang, W.; DeYonker, N. J.; Wilson, A. K., Multireference Character for 3d Transition-Metal-Containing Molecules. *J. Chem. Theory Comput.* **2012,** *8* (2), 460-8.

57. Asmis, K.; Meijer, G.; Brümmer, M.; Kaposta, C.; Santambrogio, G.; Wöste, L.; Sauer, J., Gas Phase Infrared Spectroscopy of Mono- and Divanadium Oxide Cluster Cations. *J. Chem. Phys.* **2004,** *120*, 6461-6470.

58. Santambrogio, G.; Brümmer, M.; Wöste, L.; Döbler, J.; Sierka, M.; Sauer, J.; Meijer, G.; Asmis, K. R., Gas phase vibrational spectroscopy of mass-selected vanadium oxide anions. *Phys. Chem. Chem. Phys.* **2008,** *10* (27), 3992-4005.

59. Merrick, J. P.; Moran, D.; Radom, L., An Evaluation of Harmonic Vibrational Frequency Scale Factors. *J. Phys. Chem. A* **2007,** *111* (45), 11683-11700.

60. Kashinski, D. O.; Chase, G. M.; Nelson, R. G.; Di Nallo, O. E.; Scales, A. N.; VanderLey, D. L.; Byrd, E. F. C., Harmonic Vibrational Frequencies: Approximate Global Scaling Factors for TPSS, M06, and M11 Functional Families Using Several Common Basis Sets. *J. Phys. Chem. A* **2017,** *121* (11), 2265-2273.

TOC Graphic